

NMR methods for fast data acquisition

Hanudatta S. Atreya

Abstract | NMR spectroscopy has witnessed tremendous advancements in recent years with the development of new methodologies for structure determination and availability of high-field strength spectrometers equipped with cryogenic probes. Supported by these advancements, a new dimension in NMR research has emerged which aims to increase the speed with data is collected and analyzed. Several novel methodologies have been proposed in this direction. This review focuses on the principles on which these different approaches are based with an emphasis on G-matrix Fourier transform NMR spectroscopy.

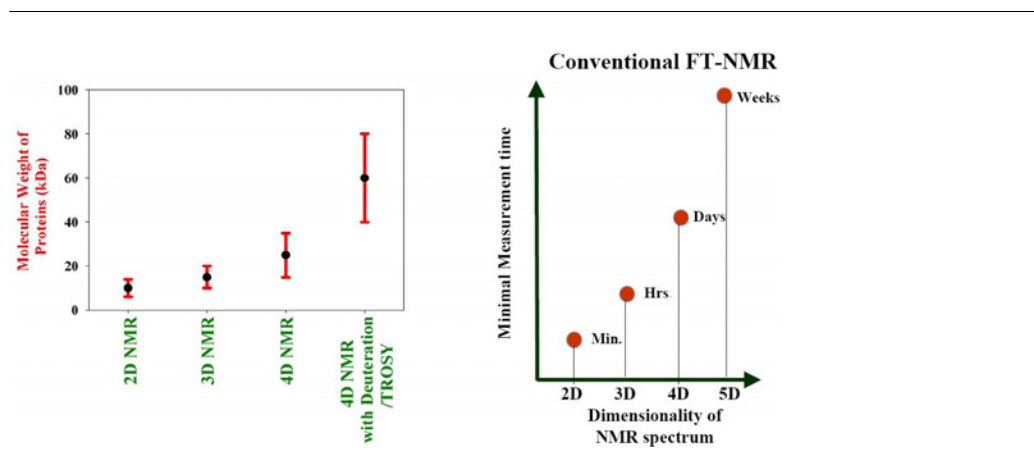
1. Introduction

One of the long-standing goals in life sciences has been to understand the mechanisms of life at the molecular level. NMR spectroscopy has played a very important role in this endeavor allowing the study of interaction between and among biomolecules and between biomolecules and ligands. Further, it facilitates three-dimensional (3D) structure determination of biomolecules in high resolution and also provides information on their dynamics at an atomic level. In recent years, NMR has witnessed tremendous advancements both in technological and methodological fronts, rendering it a powerful tool in structural biology.¹ Progress in the technique has been based on availability of large magnetic field strengths to boost sensitivity and resolution, increasingly refined probes to enhance sensitivity, reduction of the amount of sample needed for data collection and development of procedures for isotope labeling and structure determination of proteins. The size of biomolecules investigated by NMR in solution is steadily growing. Solid state NMR has also begun to contribute to the number of solved structures of proteins in the form of microcrystals, immobilized in membranes or as fibrils.¹ NMR spectroscopy has contributed immensely to structural genomics initiatives world-wide, which aim at exploring the protein 'fold space' and making available at least one

experimental structure for each family of protein sequence homologues.²⁻³

Supported by these advancements, a new dimension in NMR research has emerged which aims to increase the speed with which data is collected and analyzed.⁴⁻⁷ This is due to the fact that the conventional means of acquiring multidimensional NMR data⁸ is time-consuming: typically two-dimensional (2D) to four-dimensional (4D) NMR spectra need minutes to days, respectively, for completion, whereas five and six-dimensional (5D, 6D) experiments would be too long to be practically feasible (depicted in Figure 1). This is due to the fact that the number of acquired free inductions decays (FIDs), i.e. the number of data points sampled in the indirect dimensions, increases exponentially with increase in the number of dimensions.⁸ An ND FT NMR experiment with phase-sensitive acquisition would require sampling of $N - 1$ indirect dimensions with $n_1 \times n_2 \times \dots \times n_{N-1}$ complex points, representing $2^{N-1} \times (n_1 \times n_2 \times \dots \times n_{N-1})$ FIDs. For instance, acquiring 16 complex points in each indirect dimension (with one scan per FID each second) yields the minimal measurement time of ~ 0.5 hours for a 3D and ~ 12 days for a 5D experiment (Figure 1). Thus, two different situations arise. First, 'sensitivity-limited', when the time is set by the need to collect sufficient number of scans to obtain the

Figure 1: Schematic illustration of: (a) the type of multidimensional NMR data necessary for structural studies of proteins in different molecular weight ranges and (b) the increase in measurement time with increase in dimensionality of the NMR data.



necessary signal-to-noise ratio. Second, ‘sampling-limited’, when the length of the experiment is determined by the need to acquire a number of points in the different dimensions to obtain the required spectral resolution. With the commercial availability of high field strength magnets equipped with cryogenic RF probes, sensitivity is no longer a limitation. Most systems are thus driven into the ‘sampling-limited’ regime, where the time required for data collection becomes the rate-limiting step for structural characterization. Hence, the search for new methods for fast data collection has been actively pursued over the years.^{4–7} Rapid acquisition of multidimensional spectra also becomes important for studying slowly degrading samples and for studying various dynamic processes in biological systems with a higher time resolution. This review focuses on new developments that have taken place during the last decade in the area of rapid NMR data collection.

2. Traditional approaches to fast data collection

Traditionally, different approaches have been resorted to reduce data collection times.⁹ First, the maximum chemical shift evolution times, aq_{\max} , in the indirect dimensions can be reduced. However, this can result in truncation artifacts after data processing due to abruptly truncated FID. Practically, it is often possible to reduce aq_{\max} up to about a factor of ~ 2 . Moreover, reduction in aq_{\max} results in an increase in line widths,⁹ implying that spectral resolution and signal-to-noise ratios are reduced as a consequence of speeding up data collection. An alternative approach consists of reducing the relaxation delay between

scans, T_{recycle} . When reducing T_{recycle} , sensitivity is compromised for increased acquisition speed when relaxation delays become shorter than the longitudinal relaxation time T_1 of the nucleus being excited. This approach is further limited by the duty cycle of spectrometers in presence of broadband decoupling which is often employed for gaining sensitivity and resolution.^{8,9} A third approach consists of reducing the spectral width in the indirect dimensions so that NMR signals are aliased/folded. In protein NMR spectroscopy, signal aliasing is feasible in the aliphatic ^{13}C dimension, since $^{13}\text{C}^{\text{ali}}$ and $^1\text{H}^{\text{ali}}$ chemical shift values are strongly correlated.⁸ As a result, the spectral width in the $^{13}\text{C}^{\text{ali}}$ -dimension can be reduced up to about two to three-fold in $^{13}\text{C}^{\text{ali}}$ -resolved multidimensional experiments. Taken together, the traditional approaches for accelerating data acquisition may help reduce the measurements times up to a factor of ~ 2 , but are insufficient to compensate for the exponential increase in measurement time with the dimensionality of the experiment.

3. Modern methods for rapid data acquisition

During the last decade several new NMR methods have been proposed for increasing the speed of data collection (Table 1)^{4–7} They can be classified into six different types: (1) spatial frequency encoding approaches, (2) time sharing (simultaneous data acquisition) approach, (3) sparse sampling, (4) reduced dimensionality methods (projection NMR spectroscopy), (5) Hadamard spectroscopy and (6) fast pulsing methods. Each of these approaches are discussed below with

Table 1: List of fast NMR methods

Sr. No.	Methodology and Principle involved	Reference No
1	Ultrafast (single-scan) NMR Slice-selective excitation	11–13, 15–17, 19, 147, 154–163
2	Non-linear sampling Restricted time-domain sampling in the indirect dimension by omission of increments randomly or in a selective manner followed by spectral reconstruction.	a. Maximum Entropy Reconstruction b. Frequency Diagonalization Method c. Three-way decomposition (Multiway decomposition) 34–35, 37–39, 41, 51–52, 164–168 42–45, 169 46–48, 54, 170
3	Time-shared approach (Simultaneous Data Acquisition) Parallel execution of two or more magnetization transfer pathways in the RF pulse sequence	21, 23–24, 27
4	Projection NMR spectroscopy Phase sensitive or non-phase sensitive joint sampling of two or more chemical shifts in the indirect dimension(s)	a. RD-NMR b. GFT NMR c. GFT-based data collection followed by spectral re-construction 28, 56–61, 63, 67–68, 85, 171–174 5, 10, 69, 84, 86, 89, 93–95, 97–104, 175–176 70, 75–77, 79, 177–179
5	Hadamard NMR spectroscopy Selective excitation and encoding of phases of signals using Hadamard matrix	137–138, 180
6	Fast pulsing methods Reduction of relaxation delay period between scans	a. L-optimization b. SO-FAST NMR c. Variable relaxation delay 93, 95, 144 6, 145–151 153

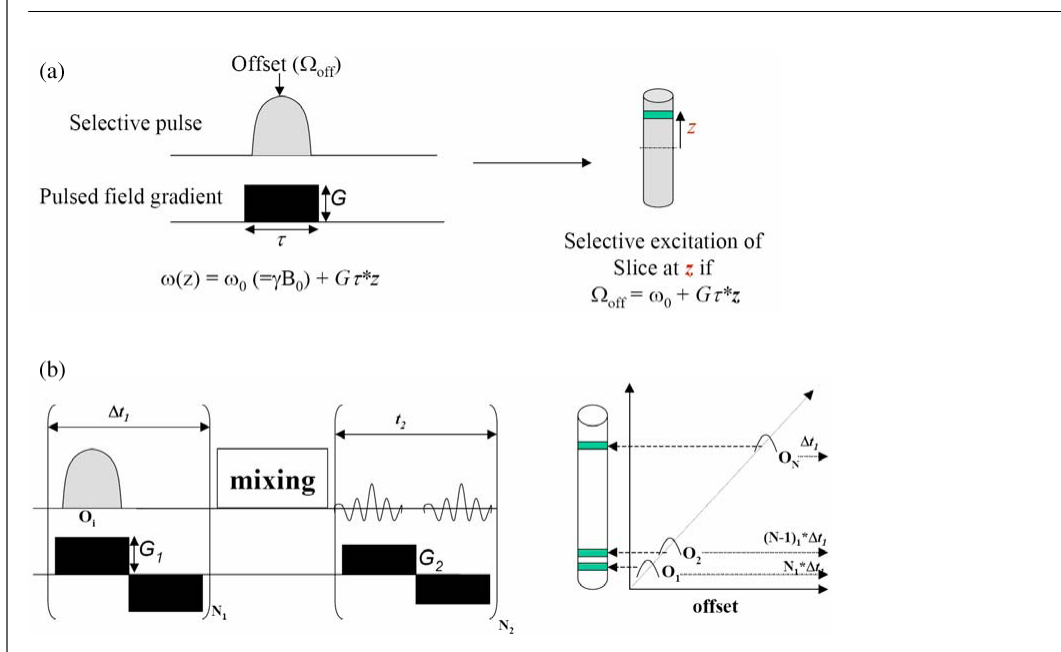
emphasis on reduced dimensionality methods, the generalization of which has been proposed in the form of G-matrix Fourier transform (GFT) projection NMR spectroscopy.¹⁰ Notably, each of the methods mentioned above use a fundamentally different approach and hence a combination of these methods can be shown to further boost the speed of data collection.

3.1. Spatial frequency encoding

Frydman et al. introduced a novel experimental scheme for the acquisition of multidimensional NMR spectra within a single scan¹¹. This method is also known as “ultrafast NMR”. The earliest proposed approach under this scheme¹¹ can be illustrated using a radio frequency (RF) pulse sequence depicted schematically in Figure 2. First, a particular ‘slice’ of a sample is selectively excited using a spatially selective RF pulse (SSP) (Figure 2a), which involves the use of pulsed field gradients (PFG) in conjunction with an amplitude/phase-modulated pulse having the desired offset (Figure 2b). Immediately afterwards a short delay period is given following which a second ‘slice’ along the sample is excited. This sequence of SSPs followed by delay periods is repeated as many number of times as the number of increments required in the indirect dimension (N_1 in Figure 2). Thus, if 128 increments are desired in the indirect dimensions, 128 slices are excited sequentially. After the end of the sequence, the first

slice would have undergone the maximum phase evolution due to the chemical shift of nuclei in that slice and the last slice would have undergone the smallest phase evolution (Figure 2b). Thus, chemical shift evolution, which in the conventional methods is encoded as phase evolution for each increment in the indirect dimension, now gets spatially encoded in different slices along the sample. These are then ‘read out’ in conjunction with the chemical shift evolution in the direct dimension (Figure 2b). All these happen within a single scan or transient, thereby avoiding multiple repetitions of the experiments to collect different increments in the indirect dimension (as done conventionally). In principle, this acquisition scheme can be extended to arbitrary number of dimensions¹². In recent years, several applications of this methodology have been proposed¹³. Reduced sensitivity, however, currently limits one to use 2D single scan acquisition for biological macromolecules. However, using the recently proposed method of dynamic nuclear polarization (DNP) in solution,¹⁴ the ultra fast single scan method has been shown to yield spectra with increased sensitivity.^{15–16} A number of applications have been proposed in recent years which can benefit from the single-scan approach such as the measurement of exchange rates of protons undergoing fast chemical exchange with solvent protons,¹⁷ measurement of longitudinal relaxation rates,¹⁸ monitoring chromatographic separations in real time,¹⁹ etc. A recent review

Figure 2: (a) Schematic illustration of slice-selective excitation using a combination of pulsed field gradient and a band-selective RF-pulse. (b) Ultrafast (single-scan) scheme of data acquisition proposed by Frydman *et al* (2002).



of this methodology covers these aspects in more detail.¹³

An elegant way to use slice selective excitation was recently shown by Szyperski and co-workers,²⁰ wherein different slices of the sample were chosen to encode the different steps of a phase cycle required in the experiment. Thus, a 4 step phase cycling comprising 0°, 90°, 180° and 270° can be implemented by dividing the sample into four slices and assigning each phase to each slice and then combining the resulting signal. This speeds up data acquisition by a factor of 4. This idea can be combined with the GFT NMR approach described below.

3.2. Time sharing/simultaneous data acquisition approach

The simultaneous acquisition of two multidimensional NMR spectra reduces data acquisition times by performing different experiments at the same time. For example, a 2D [¹⁵N, ¹H] and [¹³C, ¹H] HMQC can be acquired simultaneously because ¹H to ¹⁵N and ¹H to ¹³C polarization transfer followed by the chemical shift evolution of ¹³C/¹⁵N in the respective experiments can be accomplished simultaneously and independently. Since the protons attached to these heteronuclei have distinct chemical shifts, the two spectra can be displayed without mutual interference. Thus, two HMQC spectra

can be acquired in a single data set, reducing the measurement time by almost a factor of 2. This approach was proposed first by Falmer for 2D [¹³C-¹H]/[¹⁵N-¹H]-HMQC,²¹ followed by Boelens *et al.* (1994) for 3D ¹H/¹³C/¹⁵N triple resonance spectra²² and by Pascal *et al.* (1994) for simultaneous acquisition of 3D ¹⁵N- and ¹³C^{ali}-resolved [¹H, ¹H]-NOESY²³ Subsequently, additional schemes for simultaneous acquisition of 3D triple resonance experiments^{24–28} as well as an improved implementation for heteronuclear resolved NOESY²⁷ have been reported. Simultaneous acquisition of 3D ¹⁵N- and ¹³C^{ali}-resolved [¹H, ¹H]-NOESY^{23,27} is advantageous due to the clear spectral separation of amide and aliphatic proton chemical shifts. In addition, data analysis is facilitated for two heteronuclear NOESY experiments that are acquired in a single data set. Recently, a method for simultaneous acquisition of methyl and amide TROSY spectra for large deuterated proteins has also been proposed.²⁹ However, implementing two different magnetization transfer pathways within the same r.f. pulse scheme results in a compromise on the different delays tuned for polarization transfer. Another disadvantage of this method is that it can be applied only to specific pairs of nuclei whose magnetization transfer pathway along the RF pulse sequence can be kept independent. While the above developments have taken place using new RF

pulse schemes, a recent technological development involving the use of multiple receivers has also enabled simultaneous detection of heteronuclear correlation experiments.³⁰

3.3. Non-uniform/sparse sampling

In conventional multidimensional NMR spectroscopy, indirect evolution periods are incremented in a *linear* fashion by using a fixed delay ('increment') Δt .⁸ The length of the increment is defined by the spectral width according to the Nyquist theorem.^{8,9} One approach to reducing the total measurement time is to record a reduced number of FIDs by not sampling the evolution periods linearly (Figure 3). That is, to randomly select a limited number of time points out of the full set of increments in the indirect dimension. Such 'non-uniformly' or 'sparsely' sampled data sets cannot be transformed using the conventional fast Fourier transformation method. Other processing methods are then required to reconstruct the multidimensional NMR spectrum. Several methods have been proposed for spectral reconstruction of such sparsely sampled data sets: (1) Maximum entropy reconstruction (MER),³¹⁻⁴¹ (2) frequency diagonalization method (FDM)⁴²⁻⁴⁵ and multi-way or three-way decomposition (TWD)^{46-48,53,54} Several applications using MER or TWD have demonstrated that between 50% and 75% of the data points can be omitted from a conventional linearly sampled spectrum without necessarily sacrificing spectral resolution. We describe below the method of MER.

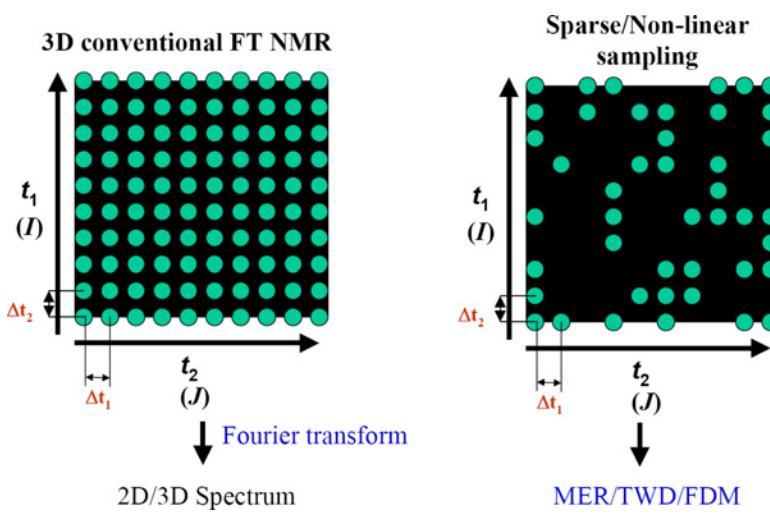
3.3.1. Maximum entropy reconstruction

Maximum entropy reconstruction of NMR spectra is based on the maximum entropy -principle: maximizing the entropy of a probability distribution yields the most uniform distribution, given a set of constraints reflecting our knowledge about the probabilities.⁴⁹ The goal of MER is to calculate the frequency domain spectrum with maximal entropy, which represents the most 'uniform' spectrum being consistent with the experimental *time* domain data^{33,50-52}. Hence, any deviation (a 'peak') from a uniform distribution (the baseline and its off-set) must originate from the experimental data serving as constraints. Mathematically, this can be achieved by maximizing the entropy and establishing consistency with experimental data, which corresponds to maximizing the target function, TF ³⁴:

$$TF(\mathbf{f}) = S(\mathbf{f}) - \lambda C(\mathbf{f}) \quad (1)$$

where \mathbf{f} represents the data points of the reconstructed spectrum, $S(\mathbf{f})$ is a measure for its entropy, $C(\mathbf{f})$ reflects the consistency of the reconstructed spectrum with the experimental data and λ is a Lagrange multiplier. The appropriate form of the entropy measure has been a subject of debate.⁵² Importantly, MER does not require *a priori* information about line shapes. However, if such information is available, it enhances the performance of MER. The same holds if uniform scalar couplings are manifested in the spectrum. Those can be considered when maximizing the

Figure 3: Schematic illustration of sparse/non-linear sampling compared to the conventional linear sampling scheme. Data processing of non-linear sampled data sets is done using either Maximum Entropy Reconstruction (MER), Three-way decomposition (TWD) or Frequency diagonalization method (FDM).



entropy, which yields a decoupled spectrum. The computational time required to recreate the spectrum by MER depends both on the number of data points and the spectral width. In the case of multidimensional NMR data, MER can be either applied sequentially or simultaneously to several dimensions. In practice, sequential application of MER is preferred due to computational requirements associated with such processing.^{34,52} One can implement non-linear sampling by probing an indirect dimension at arbitrary time points. A spacing of multiples of Δt is chosen between points, that is, the linear sampling protocol is 'diluted out' by randomly omitting a fraction of the time points of linear sampling (Figure 3). This works best for experiments with constant time chemical shift evolution periods, where the amplitude of the FID is constant³⁸. In experiments with non-constant time evolution, in order to sample at 'higher density' where the signal is stronger, it is advantageous to randomly select data points for sparse sampling in a manner that the probability of selection matches the signal envelope. Accordingly, exponentially weighted random sampling for exponentially decaying signals^{31–32} or sine-modulated exponentially weighted random sampling for signal building up according to a sine function (e.g., anti-phase signals in COSY)³⁹ have been employed. One-dimensional non-linear sampling schemes can, in principle, be combined to sample two- or possibly even higher-dimensional subspaces of a multidimensional NMR experiment in a non-linear fashion.³⁴ This would lead to a correspondingly increased acquisition speed. For example, non-linear sampling of an entire two-dimensional subspace of a ND experiment ($N > 3$) might reduce the minimal measurement time by about an order of magnitude. Future research needs to explore if multiple sparse sampling is routinely feasible.

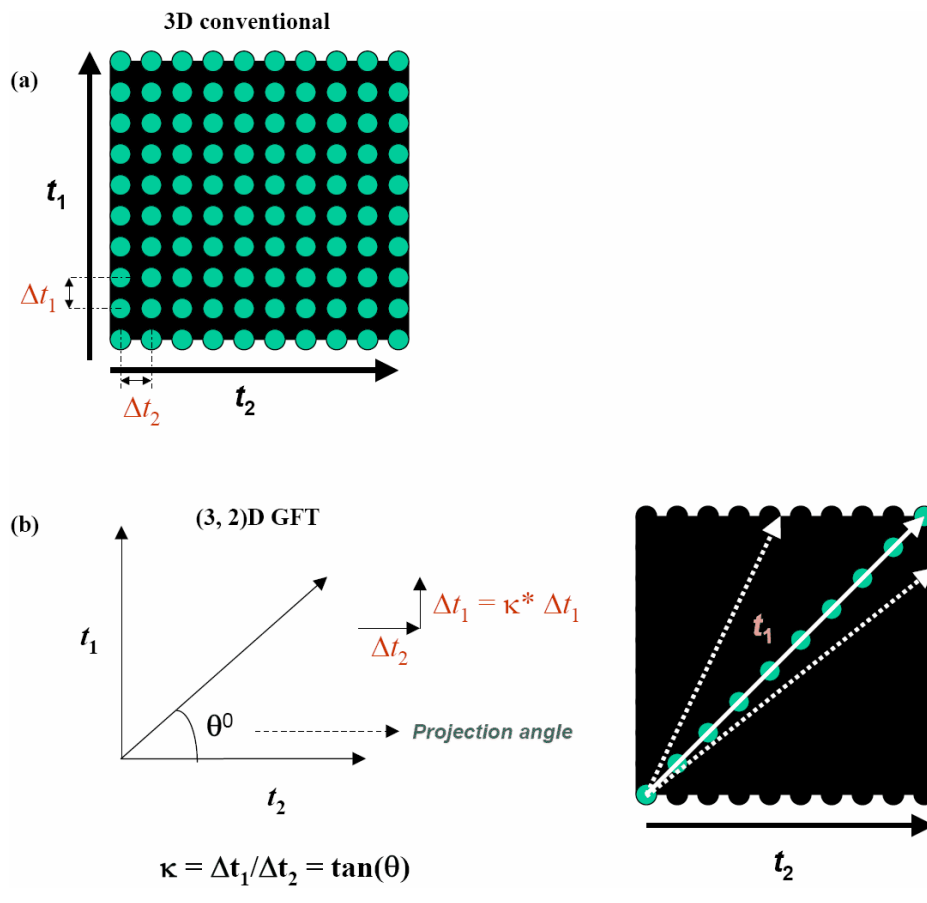
3.4. Projection NMR spectroscopy (Reduced dimensionality methods)

In view of the exponential increase of measurement time with increasing dimensionality, an attractive approach is to devise means to *encode* the information of a high-dimensional spectrum in lower spectral dimensions. This forms the basis of 'reduced-dimensionality' (RD) NMR approach proposed in the early 90s^{55–59,60–62}. The first RD NMR experiment was introduced as two-spin coherence spectroscopy and consisted of co-incrementation of two chemical shift evolution periods. In general, the RD NMR time domain sampling approach requires that the two nuclei, which are jointly sampled (i.e., their chemical

shift evolution periods are co-incremented), can be independently excited, and is thus primarily used for *projecting* multidimensional *hetero*-nuclear N dimensional (ND , with $N > 2$) chemical shift correlation spectra into an $N - 1$ dimensional subspace⁶³. Hence these methods are also known as 'projection NMR spectroscopy'.⁵⁷ One of the two jointly sampled *indirect* dimensions is detected in a phase-sensitive manner while the evolution of the second shift provides a simple cosine modulation of the transfer amplitude. This allows one to phase-sensitively detect a pair of peaks ('chemical shift doublet') located at the sum and the difference of the two jointly sampled shifts. The angle for the 'projection' can be defined by adjusting the scaling factor for the increments of the two indirect dimensions (Figure 4).⁶³ The scope of the RD NMR was expanded by introducing an approach for editing the components of the chemical shift doublet arising from the projection into two sub-spectra⁶⁴ and, as an alternative, the employment of time proportional phase incrementation (TPPI)⁶⁵ to place the components arising from the projection into distinct spectral regions.^{59,61} Further improvements were made which include the symmetrization of RD NMR spectra to increase signal-to-noise ratios^{59,61,66}, and the two-fold application of the RD NMR (the "double RD" approach) yielding a total of four components resulting from a projection of an ND spectrum into an $(N - 2)D$ space.^{67–68}

A generalization of to reduced dimensionality approach to project an ND NMR data to an $(N - K)D$ spectrum was presented as G-matrix Fourier transform (GFT) projection NMR spectroscopy. In the GFT NMR approach, joint sampling in the indirect dimension is achieved by co-incrementing two or more chemical shift evolution periods in the radio frequency (r.f.) pulse sequence, with the increments being scaled relative to each other.^{10,69} This results in signals comprising linear combination of the respective chemical shifts that are jointly sampled. The quadrature components of all the jointly sampled shifts are collected. Thus, in a generalized case of a $(N, N - K)D$ GFT NMR experiment, $K+1$ chemical shifts are jointly sampled. Out of the set of $K+1$ chemical shifts, a particular chemical shift denoted Ω_0 is chosen as the phase-sensitively detected 'center shift'. Sampling of the remaining K shifts, $\Omega_1, \Omega_2, \dots, \Omega_K$, generates chemical shift multiplets centered about Ω_0 and the linear combinations $\kappa_0\Omega_0 \pm \kappa_2\Omega_1 \dots \pm \kappa_K\Omega_K$ (projections at angles: $\pm\alpha_1, \pm\alpha_2 \dots \pm\alpha_K$) are measured. While jointly incrementing $K+1$ shift evolution periods, the phases Φ_j of the r.f. pulses exciting spins of type

Figure 4: Illustration of sampling scheme used in (a) conventional 3D experiment and (b) GFT projection NMR spectroscopy. In conventional NMR experiment, data is linearly sampled with a fixed dwell time between points. In GFT NMR, two or more chemical shifts are jointly sampled with a relative scaling factor. The projection (tilt) angles are adjusted by setting the scaling factors (κ) of the individual chemical shift evolution periods.



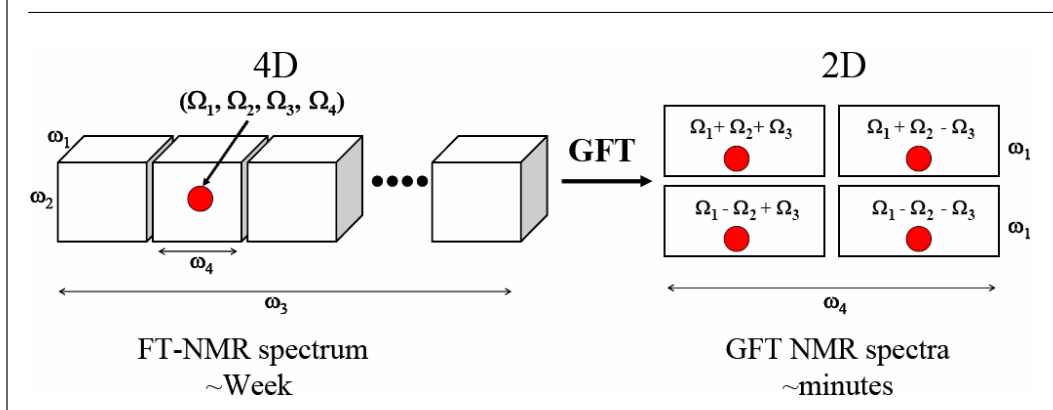
$j(j = 1 \dots K)$ are systematically varied between 0° and 90° in order to collect both cosine and sine modulated data sets. This results in 2^{K+1} FIDs, which upon G-matrix transformation yields 2^K ‘basic spectra’, and each of these sub-spectra affords editing of the shift components. To recover the full potential of the parent multidimensional NMR experiment, bottom-up identification of central peaks (located in projected planes with 0° and 90° tilt angle) can be employed¹⁰. Including the 2^K ‘basic spectra’ alluded to above, complete central peak detection requires recording of a total of $2^{K+1} - 1$ sub-spectra, which is the minimal number of sub-spectra required for resolving arbitrary $N - 1$ fold chemical shift degeneracy in a projected ND experiment. A more detailed mathematical treatment of this approach is described below (see section 3.4.1).

Recently, projected GFT subspectra, recorded with different scaling of the chemical shift

evolution periods, have been used to ‘reconstruct’ the parent ND spectrum.^{70–79} Such ‘projection-reconstruction’ (PR NMR) efforts is useful whenever manual analysis of the reconstructed ND spectrum itself is more straightforward than the analysis of the set of projections. For that purpose, the GFT NMR formalism was translated into a form, which is more readily related to the terminology used in projection-reconstruction (PR) theory.⁶⁹ In particular, the projection formalism of PR NMR is equivalent to the GFT NMR formalism and the G-matrix transformation is referred to as a (generalized) ‘hypercomplex FT’ of tilted planes in PR-NMR experiments. Among those, very recently published APSY.^{80–81} and HIFI⁸². NMR methods are significant developments towards an integrated and fully automated projection NMR spectroscopy.

By acquiring higher-dimensional spectral information in lower dimensional spectra, GFT

Figure 5: Schematic illustration of the GFT NMR scheme of data acquisition.



NMR speeds up NMR data collection by several orders of magnitude. For example, a 4D NMR experiment requiring weeks of data collection and detecting four different chemical shifts can be acquired as a 2D experiment within few hours, wherein one dimension is chosen to simultaneously encode the information of three chemical shifts (Figure 5). There are other salient features associated with the GFT NMR scheme of data collection: (i) The number of peaks in each of the sub-spectra is the same as in the original high-dimensional spectrum. This ensures that the reduction in dimensionality does not give rise to increased spectral crowding. (ii) A single dimension now encodes several different types of frequencies, resulting in higher dispersion of signals in the spectrum (e.g., linear combination of three different frequencies spans a larger spectral range than those of the individual frequencies), (ii) Chemical shifts are encoded multiple times in the linear combinations registered in GFT NMR spectra (see (Figure 5); e.g., Ω_1 , Ω_2 and Ω_3 are encoded in each of the four different GFT spectra). This is equivalent to performing statistically independent multiple measurements for a given parameter, resulting in its high precision. Moreover, there is an underlying symmetry in the peak pattern of shift multiplets, which allows one to implement robust algorithms for spectral analysis. Such features also make these experiments highly amenable to automation.^{83–84}

3.4.1. Theory of GFT NMR data acquisition, processing and analysis

If an ND FT NMR experiment is acquired as an $(N, N - K)$ D GFT NMR experiment, $K+1$ chemical shifts measured in a single ‘GFT dimension’ in which *linear combinations* of the jointly sampled shifts are detected phase-sensitively. The remaining frequency axes in the resulting $(N - K)$ D spectra

are sampled as in conventional NMR⁸. To indicate which chemical shifts are jointly sampled, the corresponding nuclei are underlined in the name of the experiments.^{56,85} For example, a 4D HNCOCA experiment can be acquired as $(4,2)$ D HNCOCA ($K = 2$), wherein the GFT dimension encodes the chemical shifts of $^{13}\text{C}^\alpha$, $^{13}\text{C}'$ and ^{15}N ($K + 1 = 3$ chemical shifts). In addition to jointly incrementing $K+1$ shifts, the phases Φ_j of the r.f. pulses exciting spins of type j ($j = 1 \dots K$) are systematically varied between 0° and 90° in order to collect both cosine and sine modulated data sets. This results in 2^K ‘basic spectra’, and G-matrix transformation of these subspectra affords editing of the shift components.

Considering that each of the 2^K subspectra contain a real and an imaginary part, a total of 2^{K+1} data sets is obtained. These can be written as a 2^{K+1} dimensional vector:

$$\mathbf{S}(j) = \begin{bmatrix} C_j \\ S_j \end{bmatrix} \quad (2)$$

$$\mathbf{S}(K) = \begin{bmatrix} C_K \\ S_K \end{bmatrix} \otimes \dots \otimes \begin{bmatrix} C_1 \\ S_1 \end{bmatrix} \otimes \begin{bmatrix} C_0 \\ S_0 \end{bmatrix} \quad (3)$$

where $c_j = \cos(\Omega_j t)$ and $s_j = \sin(\Omega_j t)$ and t defining the evolution time in the indirect GFT dimension. Multiplication of $\mathbf{S}(K)$ with the G-matrix according to:

$$\mathbf{T}(K) = \mathbf{G}(K) \cdot \mathbf{S}(K) \quad (4)$$

yields the desired vector $\mathbf{T}(K)$ which comprises the edited subspectra. The G-matrix representing a $2^K \times 2^{K+1}$ complex matrix us given as.¹⁰:

$$\mathbf{G}(K) = \begin{bmatrix} 1 & i \\ 1 & -i \end{bmatrix}_1 \otimes \dots \otimes \begin{bmatrix} 1 & i \\ 1 & -i \end{bmatrix}_K \otimes [1 \ i] \quad (5)$$

Thus, if two nuclei A and B with chemical shifts Ω_A and Ω_B are jointly sampled with relative scaling factors κ_A and κ_B , four different FIDs are collected separately with each FID having the following transfer amplitudes (Eqn. 3):

$$\begin{aligned} S_{1r} &= \cos(\kappa_A * \Omega_A * t) * \cos(\kappa_B * \Omega_B * t) \\ S_{1i} &= \sin(\kappa_A * \Omega_A * t) * \cos(\kappa_B * \Omega_B * t) \\ S_{2r} &= \cos(\kappa_A * \Omega_A * t) * \sin(\kappa_B * \Omega_B * t) \\ S_{2i} &= \sin(\kappa_A * \Omega_A * t) * \sin(\kappa_B * \Omega_B * t) \end{aligned} \Rightarrow \mathbf{S}(2)$$

$$= \begin{bmatrix} S_{1r} \\ S_{1i} \\ S_{2r} \\ S_{2i} \end{bmatrix} \quad (6)$$

These FIDs are stored separately and the application of G-matrix transformation (Eqn. 5) in a post-acquisition manner allows the editing of the linear combination of chemical shifts as follows (Eqn. 4):

$$\mathbf{G}(2) = \begin{bmatrix} 1 & 0 & 0 & -1 \\ 0 & 1 & 1 & 0 \\ 1 & 0 & 0 & 1 \\ 0 & 1 & -1 & 0 \end{bmatrix} \quad (7)$$

$$\mathbf{T}(2) = \mathbf{G}(2) \cdot \mathbf{S}(2) = \begin{bmatrix} \cos(\kappa_A \Omega_A + \kappa_B \Omega_B) t \\ \sin(\kappa_A \Omega_A + \kappa_B \Omega_B) t \\ \cos(\kappa_A \Omega_A - \kappa_B \Omega_B) t \\ \sin(\kappa_A \Omega_A - \kappa_B \Omega_B) t \end{bmatrix}$$

$$= \begin{bmatrix} e^{i(\kappa_A \Omega_A + \kappa_B \Omega_B) t} \\ e^{i(\kappa_A \Omega_A - \kappa_B \Omega_B) t} \end{bmatrix} \quad (8)$$

As a result, the 2 linear combinations $\kappa_A * \Omega_A \pm \kappa_B * \Omega_B$ (which also represent projections at angles $\pm\alpha = \tan^{-1}(\kappa_B/\kappa_A)$ (Figure 4)⁶⁹) are measured in one of each of the 2 subspectra. The principle of GFT NMR can be applied in two different indirect dimensions for two distinct sets of chemical shifts, with each set being jointly sampled. This concept resulted in the introduction of G²FT NMR spectroscopy.⁸⁶ In particular, efficient resonance assignment of polypeptide chemical shifts can be achieved by separate joint sampling of (i) chemical shifts which solely serve to provide increased resolution in one GFT dimension and (ii) shifts which also provide sequential connectivities in a second GFT dimension.

The free induction decays (FIDs) of the 2^K subspectra constituting $\mathbf{S}(K)$ (Eq. 3) are routinely recorded in an ‘interleaved manner’ as a single

data set. The subsequent G-matrix transformations (Eq. 5) are carried out with software yielding the sub-spectra, $\mathbf{T}(K)$, which are then conventionally processed using software packages such as PROSA⁸⁷ or NMRPIPE.⁸⁸

One limitation of the above method is that during each data collection, quadrature components of all the jointly sampled shifts have to be collected and stored separately. This results in an increased measurement time when only one particular or a few of the linear combination/projection out of the 2^K linear combinations is desired. In other words, even when only one of the 2^K components of the multiplet is needed, an entire data set containing information for all 2^K shift combinations is collected. For instance, in a given (4, 2)D GFT experiment, only a particular linear combination, say $\kappa_1 * \Omega_1 + \kappa_2 * \Omega_2 - \kappa_3 * \Omega_3$ (projection at an angle $(+\alpha_1, -\beta_1)$; $\alpha = \tan^{-1}(\kappa_2/\kappa_1)$ and $\beta_1 = \tan^{-1}(\kappa_3/\sqrt{(\kappa_1^2 + \kappa_2^2)})$ [3]), may be of interest and other linear combinations may not be required. Alternatively, two different linear combination such as $\kappa_1 * \Omega_1 + \kappa_2 * \Omega_2 + \kappa_3 * \Omega_3$ and $\kappa'_1 * \Omega_1 + \kappa'_2 * \Omega_2 + \kappa'_3 * \Omega_3$ ($\kappa'_1 \neq \kappa_1$; $\kappa'_2 \neq \kappa_2$; $\kappa'_3 \neq \kappa_3$) may be desired. In the above implementation, such selective detection is not possible and data has to be collected and stored for all the four (or eight) linear combinations: $\kappa_1 * \Omega_1 \pm \kappa_2 * \Omega_2 \pm \kappa_3 * \Omega_3$ (i.e., projections at angles $(\pm\alpha_1, \pm\beta_1)$) and $\kappa'_1 * \Omega_1 \pm \kappa'_2 * \Omega_2 \pm \kappa'_3 * \Omega_3$. Recently, a method was proposed based on phase cycling,⁸⁹ which releases this restriction and allows one to acquire projection NMR data comprising any given specific linear combination out of 2^K shift combinations. Instead of collecting and storing the FIDs separately, appropriate cosine/sine modulations of chemical shifts are selected and the desired linear combination is constructed by phase cycling of the radiofrequency pulses and receiver. In all the experiments, the existing 2 or more phase cycling steps in the r.f. sequence for water/artifact suppression can be utilized to incorporate this phase cycling procedure. This method, also known as Combination Shift Selective (CSC) GFT NMR, implements G-matrix transformation within the r.f. pulse sequence and hence avoids the need for any post-acquisition data processing.⁸⁹ The spectra encoding the sums and difference of chemical shifts can be directly visualized by the spectroscopist without the need of extra processing steps. The method can be applied to any projection NMR experiment employing the States method or the sensitivity-enhanced/echo-antiecho method⁹⁰ for quadrature detection.

Once the data is collected and pre-processed, analysis of the GFT NMR sub-spectra is performed as for ‘conventional’ spectra, except that one looks

at the linear combinations of chemical shifts. The G-matrix transformation ensures that all linear combinations of shifts which are of the same type are edited into the same sub-spectra, and that the number of peaks in each of the GFT sub-spectra is identical to the number in the conventional congeners of same dimensionality. Hence, the spectral dispersion increases since signals are dispersed over the sum of spectral widths. In our laboratory, XEASY,⁹¹ is used for analysis of GFT NMR spectra. Once the position of peaks in the spectra encoding the linear combination of chemical shifts is known, the shifts of individual nuclei within the shift multiplet can be obtained using the linear least square procedure.¹⁰

Furthermore, GFT NMR experiments are highly amenable to automated analysis. First, chemical shifts are measured with higher precision and accuracy than in their conventional congeners. Secondly, detection of peak patterns allows one to identify signals that are close to the noise level. The program AUTOASSIGN⁹² is used in our laboratory for protein backbone assignments using chemical shifts derived from GFT NMR spectra.

Whenever chemical shifts being detected in a constant time manner are jointly sampled, line widths are not affected by the joint sampling but are determined by the maximum evolution time of the constant-time evolution.¹⁰ However, the sensitivity of an $(N, N - K)$ D GFT experiment is reduced by a factor of $(1/\sqrt{2})^K$ compared to the parent ND experiment for the same total measurement time. This is because each additional frequency labeling results in a 2-fold decrease in sensitivity, while a factor of $\sqrt{2}$ is gained due to the fact that phase sensitive detection for one shift is excluded. This loss in intrinsic sensitivity can be at least partially recovered by symmetrization of sub-spectra about the position of central peaks, and an increase in sensitivity by a factor of about $\sqrt{2}^K$ can be expected for an $(N, N - K)$ D GFT experiment in case the symmetrization is performed in an bottom-up manner.

3.4.2. Recent developments in GFT projection NMR spectroscopy

In addition to speeding up data collection, GFT NMR has emerged as a powerful tool to address several systems in structural biology which have remained difficult to approach using traditional FT-NMR methods such as large/membrane proteins, RNA molecules, (partially) unfolded and metallo-proteins. These systems are plagued with extreme chemical shift degeneracies, precluding their efficient analysis using the available NMR methods. A number of applications of GFT NMR to different systems have been proposed in recent years.^{86,93–104} Here we review some recent applications developed in our laboratory.

3.4.2. (1) Rapid measurement of ${}^3J(H^N-H^\alpha)$ and ${}^3J(N-H^\beta)$ coupling constants in polypeptides

Measurement of three bond scalar coupling constants (3J) significantly benefits 3D structure determination of peptides and proteins.¹⁰⁵ During the last two decades, a number of NMR experiments have been proposed for the measurement of 3J in polypeptides.^{106–108} The 2D experiments suffer from error in measurement of J -couplings due to chemical shift degeneracy, line-broadening and/or limited chemical shift precision. This overlap can be reduced using 3D NMR experiments. However, their routine use in resonance assignment or/and structure determination is hampered by long 'minimal' measurement time required to acquire data with high digital resolution. We have recently proposed a set of G-matrix Fourier transform (GFT) NMR experiments overcoming these limitations and allowing rapid measurement of ${}^3J_{HNH\alpha}$ and ${}^3J_{NH\beta}$ in polypeptides.⁹⁷ Rapid and accurate measurement of these coupling constants provides opportunities to utilize them for: (i) resonance assignments, (ii) characterization of secondary structure with/without prior knowledge of resonance assignments, (iii) stereospecific assignment of prochiral groups and (iv) 3D structure determination and refinement.

The two GFT experiments: $(3,2)$ D HNHA and $(3,2)$ D HNHB are based on the method of quantitative J -correlation¹⁰⁸ for measurement of ${}^3J_{HNH\alpha}$ (Vuister and Bax 1993) and ${}^3J_{NH\beta}$,¹⁰⁹ respectively. For the nuclei shown underlined, chemical shifts are jointly sampled. Phase sensitive joint sampling of ${}^{15}\text{N}$ and ${}^1\text{H}$ chemical shifts is implemented by co-incrementing their respective chemical shift evolution periods with the ${}^1\text{H}$ shifts scaled by a factor ' κ ' relative to ${}^{15}\text{N}$.⁶⁹ This results, after G-matrix transformation, in two sub-spectra each comprising of peaks at a given linear combination of chemical shifts along the indirect dimension: $\omega_1:\Omega({}^{15}\text{N})\pm\kappa*\Omega({}^1\text{H}^\alpha)$ and $\omega_1:\Omega({}^{15}\text{N})\pm\kappa*\Omega({}^1\text{H}^N)$ in $(3,2)$ D HNHA and $\omega_1:\Omega({}^{15}\text{N})\pm\kappa*\Omega({}^1\text{H}^{\beta2/\beta3})$ and $\omega_1:\Omega({}^{15}\text{N})\pm\kappa*\Omega({}^1\text{H}^N)$ in $(3,2)$ D HNHB. The scaling factor, κ , allows one to increase the dispersion of peaks or to restrict the chemical shift evolution of ${}^1\text{H}$ to avoid loss in sensitivity due to transverse relaxation. 2D [${}^{15}\text{N}$, ${}^1\text{H}$] HSQC provides central peak information ($\omega_1:\Omega({}^{15}\text{N})$). In both $(3,2)$ D HNHA and $(3,2)$ D HNHB, the respective three-bond coupling constants are measured by taking the ratio of the intensity of peaks at $\Omega({}^{15}\text{N})\pm\kappa*\Omega({}^1\text{H}^{\alpha/\beta})$ (equivalent to 'cross peaks' in the parent 3D experiment) to $\Omega({}^{15}\text{N})\pm\kappa*\Omega({}^1\text{H}^N)$ ('diagonal peak' in the parent 3D experiment). This ratio is proportional to a function of the corresponding

scalar coupling constant.^{106,109} The (3,2)D GFT NMR experiments provide several advantages: (i) 3D spectral information can be obtained rapidly with good sensitivity. (ii) Data are acquired with high spectral/digital resolution. (iii) Spectra have high dispersion due to joint sampling of ^{15}N and ^1H shifts, which can be 'tuned' further by adjusting the scaling factor, κ . (iv) There are no 'diagonal' peaks due to detection of linear combination of ^{15}N and $^1\text{H}^N$ shifts. This allows integration of peaks, which are otherwise difficult in the 3D experiment due to overlapping diagonal peaks.¹⁰⁶

The above experiments were demonstrated for a predominantly β -sheet protein (M-crystallin; 9.5 kDa)¹¹⁰ and a predominantly α -helical protein (*EhCaBP*; 16.2 kDa).¹¹¹ These two systems were chosen to demonstrate the feasibility to different types/sizes of proteins and for the measurement of a varied range of coupling constants. The measured couplings were assessed for their accuracy by comparing them with those predicted from the Karplus relationship¹¹², using their respective NMR-derived 3D structures. The accuracy was also evaluated by comparing the coupling constants with those measured using a regular 3D HNHA and 3D HNHB experiment.

A comparison of measured $^3J_{\text{HNH}\alpha}$ couplings with those predicted from the 3D structures for residues in regular secondary structures reveals that the measured $^3J_{\text{HNH}\alpha}$ values have a root mean square deviation (r.m.s.d.) of ≤ 1.0 Hz with the predicted couplings. In addition, all $^3J_{\text{HNH}\alpha}$ values obtained from GFT spectra were compared with those obtained from a 3D HNHA, giving an r.m.s.d. of 0.6 Hz. This suggests an error of ~ 0.4 Hz for couplings measured in the GFT spectra (Assuming both GFT and its 3D congener have similar errors in couplings, $\text{r.m.s.d} = \sigma * \sqrt{2}$, where σ denotes the error of couplings measured). Rapid measurement of $^3J_{\text{HNH}\alpha}$ using (3,2)D HNHA can also facilitate a quick estimation of secondary structure content without prior knowledge of sequence specific resonance assignments. This was verified in the case of M-crystallin and *EhCaBP* by counting spin-systems that have $^3J_{\text{HNH}\alpha}$ in the range of < 5.5 Hz (α -helix), 5.5–8.0 Hz/ unobserved residues (random-coil) and > 8.0 Hz (β -sheet). The fraction of residues in these ranges were $\sim 19\%$, $\sim 41\%$, $\sim 40\%$ for M-Crystallin and $\sim 54\%$, $\sim 35\%$, $\sim 11\%$ for *Eh*-CaBP correlating well with their secondary structure (α -helix, random-coil, β -sheet) content of $\sim 12\%$, $\sim 40\%$, $\sim 48\%$ and $\sim 57\%$, $\sim 34\%$, $\sim 9\%$, respectively, based on their chemical shift indices¹¹³ and respective 3D structures. Thus, (3,2)D HNHA can benefit: (i) structural genomics projects where samples are screened to evaluate

feasibility for pursuing crystallization/NMR studies, (ii) protein-folding studies probing secondary structures in different states, and (iii) automated assignment methods utilizing information on secondary structure. On the other hand, (3,2)D HNHB provides $^1\text{H}^\beta$ shifts rapidly, which together with C^α and C^β shifts, can aid in spin system identification for resonance assignments¹¹⁴. Further, $^3J_{\text{NH}\beta}$ in the case of Ile, Thr and Val provides information on their corresponding χ_1 torsion angle. Taken together, these experiments provide new avenues for NMR-based studies of structure and folding of polypeptides.

3.4.2. (2) Rapid measurement of pseudocontact shifts in paramagnetic proteins

In recent years, pseudocontact shifts (PCSs) have emerged as important NMR parameters in calculation and refinement of high-resolution 3D structures of proteins in solution.^{115–117} These PCSs provide long-range distance information between various NMR active nuclei and the paramagnetic ion as far apart as 40 Å in 3D space.¹¹⁵ Such information is complimentary to the widely used distance constraints derived from ^1H - ^1H NOEs and hence aids in improving the quality of the resulting structures.

PCSs originate due to the presence of a paramagnetic metal centre possessing anisotropy in its electronic g-factor.¹¹⁸ A strong anisotropic dipolar interaction between the NMR active nucleus and the unpaired electron gives rise to large changes in chemical shifts of nuclei located within a specific distance of the metal-ion. From the knowledge of the 3D structure of the protein, nature of the metal ion and the assignments available under diamagnetic conditions, the PCS shifted peaks are assigned and corresponding PCSs are measured.¹¹⁵ These PCSs, in turn, are used for further refinement of the 3D structure. In many instances, spectral overlap due to line-broadening or/and increase in the number of peaks can result in ambiguities for assignments of residues that are pseudocontact shifted. In such cases, a suite of 3D triple-resonance experiments is recorded to aid in their assignment.¹¹⁵ While degeneracy in chemical shifts and the spectral overlap can be reduced using 3D NMR experiments, their utility for rapid resonance assignment and structure determination is hampered by long 'minimal' measurement time required to acquire data with high digital resolution. Further, this becomes critical if the protein under study is unstable or when the individual PCSs have to be measured with several different metal-ions. This necessitates the development of methods to speed up the process of data collection. In this

backdrop, we have proposed a novel methodology that uses a suite of NMR experiments based on the GFT NMR principle to rapidly collect the data and analyze and quantify individual PCSs of different nuclei. Four GFT NMR experiments were proposed namely, (3,2)D $\text{HN}\underline{\text{N}}\underline{\text{C}}\underline{\text{O}}$, (3,2)D $\text{HN}\underline{\text{N}}(\underline{\text{C}}\underline{\text{O}})\underline{\text{C}}\underline{\text{A}}$, (3,2)D $\text{HN}\underline{\text{N}}(\underline{\text{C}}\underline{\text{O}}\underline{\text{C}}\underline{\text{A}})\underline{\text{C}}\underline{\text{B}}$ and (3,2)D $\text{HN}\underline{\text{N}}\underline{\text{H}}\underline{\text{A}}$ facilitating the measurement of PCS of $^1\text{H}^{\text{N}}$, $^1\text{H}^{\alpha}$, $^{13}\text{C}^{\alpha}$, $^{13}\text{C}^{\beta}$, $^{13}\text{C}'$ and ^{15}N nuclei. All the proposed experiments can be acquired in a few hours time and facilitate unambiguous and accurate assignment of PCSs. Notably, the corresponding 3D experiments which can provide an *equivalent* spectral resolution would have required several fold measurement times. Figure 2 shows the four GFT (3,2)D spectra recorded on the protein calbindin.

The accuracy of the PCS values measured with the GFT spectra was evaluated by comparison with (i) PCS measured using conventional triple resonance 3D NMR experiments and ii) PCS predicted with FANTASIAN.¹¹⁹ using the high-resolution 3D structure of Calbindin as the reference. One can compare the precision of measurements for each type of PCS by considering that $\text{r.m.s.d.} = \sqrt{\sigma^2(\text{GFT}) + \sigma^2(\text{conventional})}$, where σ denotes the error/standard deviation of PCS measured. Assuming both GFT and its 3D congener have similar errors in PCS, $\text{r.m.s.d.} = \sigma * \sqrt{2}$. Based on this, a precision (σ) of 0.03–0.2 ppm is obtained for the measurement of different PCS. Measuring the PCS with high precision and accuracy renders them useful for 3D structure refinement protocols employing PCS where the accuracy of the structure depends critically on the accuracy of the calculated alignment tensor.

3.4.2. (3) Identification of C-terminal neighbors of amino acid residues without an aliphatic $^{13}\text{C}^{\gamma}$ as an aid to NMR assignments in proteins

One of the time consuming step in structure determination of proteins by NMR spectroscopy is the process of sequence specific resonance assignments.¹⁰⁵ This step involves the identification and assignment of resonances in a NMR spectrum to a specific amino acid residue in the protein from where it originates. During the last two decades, several double and triple resonance experiments have been proposed to carry out sequence specific ^1H , ^{13}C , and ^{15}N NMR assignments in isotope labeled proteins (Bax and Grzesiek 1993; Sattler et al. 1999). We have developed a new GFT NMR experiment, which provides spectral signatures for rapid identification of the specific amino acid residues. The experiment is named ACS-(3,2)D $\underline{\text{C}}\underline{\text{B}}(\underline{\text{C}}\underline{\text{A}}\underline{\text{C}}\underline{\text{O}})\underline{\text{N}}\underline{\text{H}}\underline{\text{N}}$ and ACS-DNG-(3, 2)D $\underline{\text{C}}\underline{\text{B}}(\underline{\text{C}}\underline{\text{A}}\underline{\text{C}}\underline{\text{O}})\underline{\text{N}}\underline{\text{H}}\underline{\text{N}}$, where the letters A, C, S, D, N

and G stand for the single letter code of amino acids and for the nuclei shown underlined, chemical shifts are jointly sampled. This experiment helps to rapidly identify six amino acids, namely, Ala, Cys, Ser, Asp, Asn and Gly. Further, the experiment can distinguish the redox state of Cys residues. The proposed experiment in its two forms will have wide range of applications in resonance assignment strategies and structure determination of proteins.

3.4.2. (4) GFT NMR based chemical shift editing of methyl groups

High-resolution structure determination of proteins by NMR spectroscopy primarily relies on a large network of ^1H - ^1H NOEs which provide long range distance information or distance constraints between amino acids located close in 3D space but far apart along the polypeptide chain.¹⁰⁵ A majority of these constraints are comprised of methyl-methyl and methyl-non-methyl protons.¹²⁰ This is because methyl groups constitute the hydrophobic core of globular proteins and come close in space to other methyl groups or hydrophobic groups, which are buried in the core of proteins. Further, fast rotation of the methyl protons coupled with three chemically equivalent protons renders them very sensitive compared to other protons making them favorable probes for structure determination.^{121–123} In recent years, a number of methods have been developed to exploit these characteristics of methyl protons for structural and dynamic studies in large molecular weight proteins.^{54, 120, 124–131}

In methyl groups (of Ala, Ile, Leu, Met, Thr and Val) there is a significant overlap of ^{13}C and ^1H chemical shifts.¹³² Typically, the ^{13}C and ^1H shifts fall in the range of 5–25 ppm and 0–1.5 ppm, respectively, for all methyl group containing amino acids. This overlap is aggravated in multidimensional NMR experiments (specifically a 3D experiment), where one 2D projection happens to contain ^{13}C - ^1H correlations. A 4D experiment containing an additional ^{13}C dimension can help resolve such overlap.¹³³ However, the long minimal measurement time of 4D NMR experiments precludes their use for routine structural analysis. We have recently developed a GFT NMR experiment, which overcomes this limitation and facilitates rapid acquisition of spectra with high resolution.⁹⁹ The experiment, namely, methyl edited (3,2)D $\underline{\text{H}}\underline{\text{C}}\underline{\text{C}}\underline{\text{H}}$ -COSY exploits the fact that while the ^{13}C chemical shifts of the different methyl groups overlap, the directly one-bond attached neighboring carbon nucleus of the respective methyl groups have distinct ^{13}C chemical shifts for the different amino acid types. Thus, for instance, $^{13}\text{C}^{\alpha}$ of alanine, which is directly attached to its methyl carbon, $^{13}\text{C}^{\beta}$, has a

distinct chemical shift than $^{13}\text{C}^\beta$ of threonine which is directly attached to its methyl carbon, $^{13}\text{C}^\gamma$. Thus, an experiment, which couples the chemical shift of a methyl carbon with its directly attached neighboring carbon nuclei can facilitate the distinction between the different methyl groups, which otherwise overlap in their ^{13}C and ^1H chemical shift. This forms the basis of GFT methyl edited (3,2)D HCCH-COSY experiment.⁹⁹ This experiment was demonstrated for stereo specific assignment of methyl groups of leucine and Valine.

One promising application of this experiment is its utilization in NOESY experiments to provide distance constraints between methyl groups and other protons constituting the hydrophobic core of the protein. Currently, a 3D ^{13}C -edited ^1H - ^1H NOESY and/or 4D ^{13}C - ^{13}C NOESY is used for this purpose. However, due to overlap of ^{13}C and ^1H chemical shifts of methyl groups, the 2D projection in these experiments containing ^{13}C - ^1H correlations exhibit significant overlap. Such overlap can be resolved if the experiment is implemented in a way that GFT methyl edited (3,2)D HCCH becomes one of the 2D projections of the 3D experiment. Thus, a GFT (4,3)D NOESY-HCCH experiment can provide significant resolution beneficial for large molecular weight proteins. Design and implementation of such an experiment is currently in progress in our laboratory.

3.4.2. (5) Secondary structure type editing, assignment and estimation in proteins using linear combination of chemical shifts (CSSI-PRO)

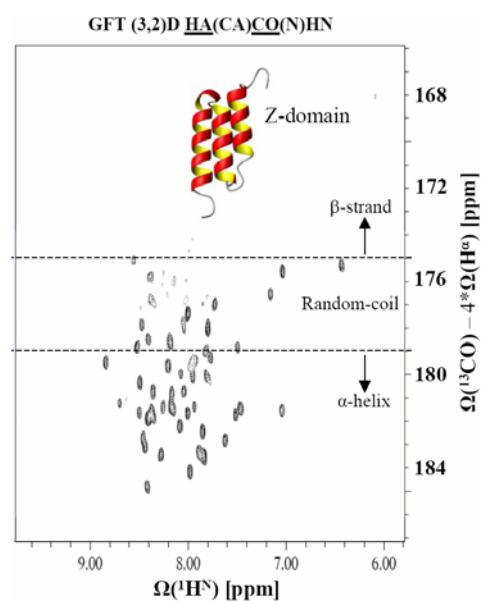
Estimation of secondary structure in polypeptides is important for studying their structure, folding and dynamics. In NMR spectroscopy, such information is generally obtained after sequence specific resonance assignments are completed. Currently, three methods are used widely to obtain this information: (1) the method of chemical shift index (CSI), wherein, the deviation of the observed chemical shift of a given residue from its random-coil value provides information on its secondary structure^{113,134–135} (Wishart and Sykes, 1994), (2) the method based on the observation of specific pattern/intensity of cross peaks in the NMR spectrum obtained using nuclear Overhauser effect spectroscopy (NOESY)¹⁰⁵ and (3) the value of three bond scalar coupling constant ($^3J_{HH}^{N\alpha}$) involving backbone dihedral angle, φ , which correlates with the secondary structure.^{97,105,112} Using these methods, the various secondary structural elements in a given protein is determined *after* the process of sequence specific resonance assignments is completed.

We have recently proposed a new methodology for assignment of secondary structure type to spin systems in proteins directly from NMR spectra, without prior knowledge of resonance assignments¹⁰² The methodology, named CSSI-PRO (Combination of Shifts for Secondary Structure Identification in PROteins), involves detection of specific linear combination of backbone $^1\text{H}^\alpha$ and $^{13}\text{C}'$ chemical shifts in a two-dimensional (2D) NMR experiment based on G-matrix Fourier transform (GFT) NMR spectroscopy¹⁰² Such linear combinations of shifts facilitate editing of residues belonging to α -helical / β -strand regions into distinct spectral regions nearly independent of the amino acid type, thereby allowing the estimation of overall secondary structure content of the protein. The experiments specifically devised is a GFT (3,2)D HA(CA)CO(N)H. Figure 6 illustrates this methodology for a predominantly α -helical protein, Z-domain.

3.5. Hadamard NMR spectroscopy

Multidimensional NMR data acquisition can be accelerated if the resonance lines have distinct chemical shift ranges in the spectrum and can be excited with selective r.f. pulses.^{136–138} Hadamard NMR spectroscopy is based on selective excitation of NMR lines and their encoding in the form of a 'Hadamard matrix' (Bolinger and Leigh, 1988; Goelman et al., 1990). The experiment is carried out

Figure 6: GFT (3,2)D HA(CA)CO(N)HN spectra recorded for the predominantly alpha-helical protein, Z-domain (M, ~ 6 kDa) for estimation of secondary structure using the methodology of CSSI-PRO.¹⁰² The 3D structure of the protein is shown in the inset. The different regions of the spectrum corresponding to the different secondary structures are indicated.



using set of N selective pulses irradiating N different regions of the spectrum simultaneously. The phases of the individual selective pulses are then varied in a series of scans, that is, they are encoded based on a Hadamard matrix of order N in each of the successive scans. Linearly combining the responses from all N scans ('Hadamard transformation') enables one to separate the N individual responses. The selective irradiation scheme with Hadamard encoding can be applied to either the excitation pulses or to spin inversion pulses.

3.6. Fast pulsing methods

As mentioned in the beginning, one approach adopted for fast data acquisition of multidimensional NMR is the reduction of relaxation delay between scans. This is because the relaxation delay (~ 1 s) is 10–20 fold longer than the sum of pulse sequence duration and acquisition time in the direct dimension^{8–9}. Thus, a substantial amount of time is invested for the allowing the system to return to equilibrium and considerable time can be saved if this delay is reduced. However, a simple shortening of this duration is not the solution since the signal-to-noise is reduced significantly due to incomplete recovery of magnetization to equilibrium. Different methodologies have been developed to speed up the recovery of the magnetization. There are three fundamentally different approaches: (1) use of paramagnetic impurities, (2) longitudinal ^1H relaxation optimization and (3) use of Ernst angle for excitation.

3.6.1. Use of paramagnetic impurities to reduce T_1

Paramagnetic metal ions containing an unpaired electron have been used in recent years to study enhancement of relaxation rates in proteins for structure determination.^{139–140} The high gyromagnetic ratio of electrons compared to the nucleons renders their dipolar interactions with the nuclei extremely efficient for relaxation. The presence of paramagnetic ions leads to reduction of both T_1 and T_2 relaxation times of NMR active nuclei located in close vicinity of the metal ion. A reduction of T_1 is beneficial for fast data acquisition as the relaxation delay period between scans required for recovery of magnetization to equilibrium can be reduced. In recent years, this methodology has been developed to enhance data collection speeds.^{141–142} However, addition of paramagnetic ions can also shorten T_2 , which can result in line broadening and reduced sensitivity. Hence, an appropriate choice of the metal ion has to be made. A more elegant way to reduce T_1 is the method of longitudinal ^1H relaxation optimization, which is described next.

3.6.2. Longitudinal ^1H relaxation optimization

In triple resonance experiments involving the excitation and detection of amide protons ($^1\text{H}^N$), the water proton magnetization is usually preserved along $+z$ -axis with minimal perturbation so as to avoid saturation of $^1\text{H}^N$ exchanging rapidly with water protons.¹⁴³ Pervushin and co-workers recently proposed that the rate of recovery of $^1\text{H}^N$ to equilibrium could be enhanced if, in addition to the water protons, the aliphatic protons are also preserved (with minimal perturbation) along $+z$ -axis before detection.¹⁴⁴ This is known as longitudinal ^1H relaxation optimization (also referred to as L-optimization). The rapid relaxation of $^1\text{H}^N$ arises from dipolar coupling of the amide protons with that of the neighbouring aliphatic protons. This requires that the amide protons have sufficiently high density of aliphatic protons surrounding them. This is usually not a problem in proteins having a well-folded conformation, which have a dense network of closely spaced ^1H atoms. Upto a factor 5.0 or more reduction in the relaxation-delay can be achieved using this method. In the case of deuterated proteins, enhancement of T_1 relaxation rate is not possible due to weaker dipolar coupling of amide protons with surrounding deuterons. Owing to the fact that both aliphatic and water protons are preserved along z -axis necessitates the use of band selective pulses which are either selective on the amide protons or on the water/aliphatic protons. Practically the easier approach is to modify the water selective 'flip-back' pulse usually present in the triple resonance experiments to preserve water proton magnetization along $+z$ -axis to also include the aliphatic protons, which usually resonate 3–4 ppm upfield of the amide protons.

L-optimization was first demonstrated as an excellent tool to speed up GFT-projection NMR spectroscopy for amide detected out-and-back type of triple resonance experiments⁹³ and for experiments involving aromatic protons.⁹⁵ Subsequently, this methodology was incorporated in the SOFAST-NMR experiments^{6, 145–151} in conjunction with Ernst angle excitation⁹ to speed up data collection.

3.6.3. Use of Ernst angle while reducing relaxation delay

The Ernst angle approach involves choosing an appropriate flip angle of an excitation pulse so as to maximize the signal recovery.⁹ This is based on the fact that the recovery of longitudinal magnetization during the relaxation delay between scans is usually not complete and after a few repetitions, a steady state is established. The maximum signal amplitude

is then no longer obtained for a flip angle of 90° for the excitation pulse but for an angle, $\cos(\alpha_{\text{opt}}) = \exp(-T/T_1)$, where T is the relaxation delay and T_1 is the longitudinal relaxation time.⁹ Thus by adjusting the pulse rotation angle (which will lead to maximum signal recovery), shorter relaxation delays can be used. This was initially shown by Ross et al. for recording fast 2D HMQC¹⁵² and later used by Brutscher et al. in SO-FAST HMQC experiments.^{6, 145–151}

3.6.4. Use of variable relaxation/recycle delay

In all the methods described up to now the delay period for the recovery of magnetization to equilibrium between scans is kept constant throughout the experiment. Macura recently demonstrated a method that employs a variable relaxation delay period between scans.¹⁵³ The basis of this method is that many a times multidimensional NMR experiments comprise truncated FIDs and hence require that the signal be apodized in all the dimensions using a suitable filter function before Fourier transformation. This apodization scales down the later part of the signal. Instead of scaling the signal down after data acquisition, the experiment can be implemented in such a way that the signal itself decays to zero towards the end to avoid any truncation artefacts. This can be achieved if the relaxation delay between scans is gradually decreased as the experiment proceeds such the magnetization does not recover back to equilibrium completely and the signal intensity gets reduced, thereby mimicking an apodization process. Reducing the relaxation between scans increases the data acquisition speed. This method was demonstrated both on a small molecule and the protein Ubiquitin.¹⁵³ One drawback of this method is that while the signal intensity is reduced as the experiment proceeds, the noise during the detection period remains the same. Thus, the signal-to-noise ratio is reduced. This does not happen in the conventional experiments because apodization affects both the signal and the noise and hence the signal-to-noise ratio is not compromised.

4. Conclusions and future prospects

As alluded to above, the different methods for rapid data collection use fundamentally different approaches and hence can be combined together to further boost data collection. For example, L-optimization was shown to speed up data acquisition by combining it with the GFT NMR approach.⁹³ Recently, the ultrafast NMR method was combined with: (1) GFT scheme of data acquisition,¹⁵⁴ (2) SO-FAST NMR method¹⁴⁷ and

(3) Hadamard NMR spectroscopy.¹⁵⁵ In another application, Hadamard scheme of data acquisition was coupled with the SO-FAST NMR method.¹⁴⁵ Thus, while new methods continue to be developed, experiments developed in the future can combine the different approaches to gain unprecedented speed in data collection. This can benefit studies such protein folding, where monitoring the folding process in real time remains a challenge as the whole process is completed within milliseconds time scale, whereas the fastest possible NMR methods require about ~ 1 s to complete data collection.

All fast NMR methods are applicable to systems, which are sampling limited. Any reduction in measurement time concomitantly leads to reduction in sensitivity because the overall sensitivity is proportional to the square root of the measurement time. Application of these methods to large molecular proteins and/or samples with low concentration which are sensitivity-limited systems will be possible in near future due to the availability of high field spectrometers equipped with cryogenic probes. The method of DNP^{14–15} holds promise for further boosts in sensitivity and will be used in future for application of fast NMR methods to sensitivity limited systems.

Almost all of the fast NMR methods have been applied up to now to solution state NMR studies of small molecules and biomolecules such as proteins. Solid state NMR spectroscopy is rapidly emerging as a tool for structural studies of biomolecules. One limitation, which slows down acquisition of multidimensional NMR experiments in the solid state, is the long phase cycling steps required for reducing the artefacts. These experiments will benefit from fast NMR methods. Moreover, application of fast methods for nucleic acids has not been proposed. Some applications in this direction are awaited.

In conclusion, fast data acquisition methods have revolutionized NMR spectroscopy. It is leading to a paradigm shift in NMR and will significantly influence future NMR studies replacing soon the conventional methods of data collection. It is reminiscent of the early days of protein structure determination by NMR, which was viewed with a lot of scepticism. However, NMR based peptide and protein structure determination is now a well-established method.

Acknowledgements

Support from Department of Atomic Energy (DAE) BRNS and DST-SERC research awards and the facilities provided by NMR Research Centre at IISc supported by DST is gratefully acknowledged.

Received 14 December 2009; accepted 20 December 2009.

References

1. Wüthrich, K. *Nature Struct. Biol.*, **5**, 492–95 (1998).
2. Montelione, G. T., Zheng, D. Y., Huang, Y. P. J., Gunsalus, K. C. and Szyperski, T. *Nature Struct. Biol.*, **7**, 982–85 (2000).
3. Yee, A., Gutmanas, A. and Arrowsmith, C. H. *Curr. Opin. Struct. Biol.*, **16**, 611–17 (2006).
4. Freeman, R. and Kupce, E. *J. Biomol. NMR*, **27**, 101–13 (2003).
5. Atreya, H. S. and Szyperski, T. *Methods Enzymol.*, **394**, 78–108 (2005).
6. Schanda, P. *Prog. NMR Spectrosc.*, **55**, 238–65 (2009).
7. Felli, I. C. and Brutscher, B. *Chem Phys Chem*, **10**, 1356–68 (2009).
8. Cavanagh, J., Fairbrother, W. J., Palmer, A. G. and Skelton, N. J. *Protein NMR Spectroscopy*; Academic Press: San Diego, CA, 1996.
9. Ernst, R. R., Bodenhausen, G. and Wokaun, A. *Principles of Nuclear Magnetic Resonance in one and two Dimensions*; Oxford Univ. Press: Oxford, 1987.
10. Kim, S. and Szyperski, T. *J. Am. Chem. Soc.*, **125**, 1385–93 (2003).
11. Frydman, L., Scherf, T. and Lupulescu, A. *Proc. Natl. Acad. Sci. USA*, **99**, 15858–62 (2002).
12. Shrot, Y. and Frydman, L. *J. Am. Chem. Soc.*, **125**, 11385–96 (2003).
13. Mishkovsky, M. and Frydman, L. *Ann. Rev. Phys. Chem.*, **60**, 429–48 (2009).
14. Ardenkjær-Larsen, J. H., Fridlund, B., Gram, A., Hansson, G., Hansson, L., Lerche, M. H., Servin, R., Thaning, M. and Goldman, K. *Proc. Natl. Acad. Sci.*, **100**, 10158–63 (2003).
15. Frydman, L. and Blazina, D. *Nature Physics*, **3**, 415–19 (2007).
16. M., M. and L., F. *Chem. Phys. Chem*, **16**, 2340–48 (2008).
17. Gal, M., Mishkovsky, M. and Frydman, L. *J. Am. Chem. Soc.*, **128**, 951–56 (2006).
18. Bhattacharyya, R. and Kumar, A. *Chem. Phys. Lett.*, **383**, 99–103 (2004).
19. Shapira, B., Karton, A., Aronzon, D. and Frydman, L. *J. Am. Chem. Soc.*, **126**, 1262–65 (2004).
20. Parish, D. M. and Szyperski, T. *J. Am. Chem. Soc.*, **130**, 4925–33 (2008).
21. Falmer, B. T. *J. Magn. Reson.*, **93**, 635–41 (1991).
22. Boelens, R., Burgering, M., Fogh, R. H. and Kaptein, R. *J. Biomol. NMR*, **4**, 201–13 (1994).
23. Pascal, S. M., Muhandiram, D. R., Yamazaki, T., Formankay, J. D. and Kay, L. E. *J. Magn. Reson. Series B*, **103**, 197–201 (1994).
24. Mariani, M., Tessari, M., Boelens, R., Vis, H. and Kaptein, R. *J. Magn. Reson.*, **B104**, 294–97 (1994).
25. Pang, Y. X., Zeng, L., Kurochkin, A. V. and Zuiderweg, E. R. P. *J. Biomol. NMR*, **11**, 185–90 (1998).
26. Hu, W. D., Gosser, Y. Q., Xu, W. J. and Patel, D. J. *J. Biomol. NMR*, **20**, 167–72 (2001).
27. Xia, Y. L., Yee, A., Arrowsmith, C. H. and Gao, X. L. *J. Biomol. NMR*, **27**, 193–203 (2003).
28. Xia, Y. L., Arrowsmith, C. H. and Szyperski, T. *J. Biomol. NMR*, **24**, 41–50 (2002).
29. Guo, C., Zhang, D. and Tugarinov, V. *J. Am. Chem. Soc.*, **130**, 10872–73 (2008).
30. Kupce, E., Cheatham, S. and Freeman, R. *Mag. Reson. Chem.*, **45**, 378–80 (2007).
31. Barna, J. C. J. and Laue, E. D. *J. Magn. Reson.*, **75**, 384–89 (1987).
32. Barna, J. C. J., Laue, E. D., Mayger, M. R., Skilling, J. and Worrall, S. J. *J. Magn. Reson.*, **73**, 69–77 (1987).
33. Sibisi, S., Skilling, J., Brereton, R. G., Laue, E. D. and Staunton, J. *Nature*, **311**, 446–47 (1984).
34. Hoch, J. C. and Stern, A. S. In *Nuclear Magnetic Resonance of Biological Macromolecules*, pt a, 2001; Vol. 338.
35. Hoch, J. C., Stern, A. S., Donoho, D. L. and Johnstone, I. M. *J. Magn. Reson.*, **86**, 236–46 (1990).
36. Mobli, M., Stern, A. S. and Hoch, J. C. *J. Magn. Reson.*, **182**, 96–105 (2006).
37. Rovnyak, D., Frueh, D. P., Sastry, M., Sun, Z. Y. J., Stern, A. S., Hoch, J. C. and Wagner, G. *J. Magn. Reson.*, **170**, 15–21 (2004).
38. Schmeider, P., Stern, A. S., Wagner, G. and Hoch, J. C. *J. Biomol. NMR*, **4**, 483–90 (1994).
39. Schmieder, P., Stern, A. S., Wagner, G. and Hoch, J. C. *J. Biomol. NMR*, **3**, 569–76 (1993).
40. Shimba, N., Stern, A. S., Craik, C. S., Hoch, J. C. and Dotsch, V. *J. Am. Chem. Soc.*, **125**, 2382–83 (2003).
41. Stern, A. S., Li, K. B. and Hoch, J. C. *J. Am. Chem. Soc.*, **124**, 1982–93 (2002).
42. Armstrong, G. S., Cano, K. E., Mandelshtam, V. A., Shaka, A. J. and Bendiak, B. *J. Magn. Reson.*, **170**, 156–63 (2004).
43. Armstrong, G. S., Mandelshtam, V. A., Shaka, A. J. and Bendiak, B. *J. Magn. Reson.*, **173**, 160–68 (2005).
44. Chen, J. H., De Angelis, A. A., Mandelshtam, V. A. and Shaka, A. J. *J. Magn. Reson.*, **162**, 74–89 (2003).
45. Chen, J. H., Nietlispach, D., Shaka, A. J. and Mandelshtam, V. A. *J. Magn. Reson.*, **169**, 215–24 (2004).
46. Korzhnev, D. M., Ibraghimov, I. V., Billeter, M. and Orekhov, V. Y. *J. Biomol. NMR*, **21**, 263–68 (2001).
47. Orekhov, V. Y., Ibraghimov, I. V. and Billeter, M. *J. Biomol. NMR*, **20**, 49–60 (2001).
48. Orekhov, V. Y., Ibraghimov, I. and Billeter, M. *J. Biomol. NMR*, **27**, 165–73 (2003).
49. Jaynes, E. T., Ed., *Where do we stand on maximum entropy?*, MIT Press: Cambridge, 1979.
50. Sibisi, S. *Nature*, **301**, 134–36 (1983).
51. Hoch, J. C. *J. Magn. Reson.*, **64**, 436–40 (1985).
52. Hoch, J. C. *Methods Enzymol.*, **176**, 216–41 (1989).
53. Ibraghimov, I. *Numerical Linear Algebra with Applications*, **9**, 551–65 (2002).
54. Tugarinov, V., Kay, L. E., Ibraghimov, I. and Orekhov, V. Y. *J. Am. Chem. Soc.*, **127**, 2767–75 (2005).
55. Szyperski, T., Güntert, P., Stone, S. R. and Wüthrich, K. *J. Mol. Biol.*, **228**, 1193–205 (1992).
56. Szyperski, T., Wider, G., Bushweller, J. H. and Wüthrich, K. *J. Am. Chem. Soc.*, **115**, 9307–08 (1993).
57. Szyperski, T., Pellecchia, M. and Wüthrich, K. *J. Magn. Reson. Series B*, **105**, 188–91 (1994).
58. Szyperski, T., Wider, G., Bushweller, J. H. and Wüthrich, K. *J. Am. Chem. Soc.*, **116**, 1601–01 (1994).
59. Szyperski, T., Braun, D., Fernandez, C., Bartels, C. and Wüthrich, K. *J. Magn. Reson. Series B*, **108**, 197–203 (1995).
60. Simorre, J. P., Brutscher, B., Caffrey, M. S. and Marion, D. *J. Biomol. NMR*, **4**, 325–33 (1994).
61. Brutscher, B., Cordier, F., Simorre, J. P., Caffrey, M. and Marion, D. *J. Biomol. NMR*, **5**, 202–06 (1995).
62. Morelle, N., Brutscher, B., Simorre, J. P. and Marion, D. *J. Biomol. NMR*, **5**, 154–60 (1995).
63. Szyperski, T., Yeh, D. C., Sukumaran, D. K., Moseley, H. N. B. and Montelione, G. T. *Proc. Natl. Acad. Sci. USA*, **99**, 8009–14 (2002).
64. Brutscher, B., Morelle, N., Cordier, F. and Marion, D. *J. Magn. Reson. Series B*, **109**, 238–42 (1995).
65. Marion, D. and Wüthrich, K. *Biochemical and Biophysical Research Communications*, **113**, 967–74 (1983).
66. Szyperski, T., Braun, D., Banerji, B. and Wüthrich, K. *J. Am. Chem. Soc.*, **118**, 8146–47 (1996).
67. Löhr, F. and Rüterjans, H. *J. Biomol. NMR*, **6**, 189–97 (1995).
68. Ding, K. Y. and Gronenborn, A. M. *J. Magn. Reson.*, **156**, 262–68 (2002).
69. Szyperski, T. and Atreya, H. S. *Mag. Reson. Chem.*, **44**, S51–S60 (2006).
70. Kupce, E. and Freeman, R. *J. Biomol. NMR*, **27**, 383–87 (2003).

71. Kupce, E. and Freeman, R. *J. Am. Chem. Soc.*, **126**, 6429–40 (2004).
72. Kupce, E. and Freeman, R. *Spectroscopy*, **19**, 16–20 (2004).
73. Freeman, R. and Kupce, E. *Current Analytical Chemistry*, **2**, 101–05 (2006).
74. Yoon, J. W., Goddill, S., Kupce, E. and Freeman, R. *Magn. Reson. Chem.*, **44**, 197–209 (2006).
75. Coggins, B. E., Venters, R. A. and Zhou, P. *J. Am. Chem. Soc.*, **126**, 1000–01 (2004).
76. Coggins, B. E., Venters, R. A. and Zhou, P. *J. Am. Chem. Soc.*, **127**, 11562–63 (2005).
77. Venters, R. A., Coggins, B. E., Kojetin, D., Cavanagh, J. and Zhou, P. *J. Am. Chem. Soc.*, **127**, 8785–95 (2005).
78. Jiang, L., Coggins, B. E. and Zhou, P. *J. Magn. Reson.*, **175**, 170–76 (2005).
79. Coggins, B. E. and Zhou, P. *J. Biomol. NMR*, **34**, 179–95 (2006).
80. Hiller, S., Fiorito, F., Wuthrich, K. and Wider, G. *Proc. Natl. Acad. Sci. USA*, **102**, 10876–81 (2005).
81. Hiller, S., Wider, G. and Wuthrich, K. *J. Biomol. NMR*, **42**, 179–95 (2008).
82. Eghbalnia, H. R., Bahrami, A., Tonelli, M., Hallenga, K. and Markley, J. L. *J. Am. Chem. Soc.*, **127**, 12528–36 (2005).
83. Moseley, H. N. B., Riaz, N., Aramini, J. M., Szyperski, T. and Montelione, G. T. *J. Magn. Reson.*, **170**, 263–77 (2004).
84. Liu, G. H., Shen, Y., Atreya, H. S., Parish, D., Shao, Y., Sukumaran, D. K., Xiao, R., Yee, A., Lemak, A., Bhattacharya, A., Acton, T. A., Arrowsmith, C. H., Montelione, G. T. and Szyperski, T. *Proc. Natl. Acad. Sci. USA*, **102**, 10487–92 (2005).
85. Szyperski, T., Wider, G., Bushweller, J. H. and Wuthrich, K. *J. Biomol. NMR*, **3**, 127–32 (1993).
86. Atreya, H. S., Eletsy, A. and Szyperski, T. *J. Am. Chem. Soc.*, **127**, 4554–55 (2005).
87. Güntert, P., Dotsch, V., Wider, G. and Wuthrich, K. *J. Biomol. NMR*, **2**, 619–29 (1992).
88. Delaglio, F., Grzesiek, S., Vuister, G. W., Zhu, G., Pfeifer, J. and Bax, A. *J. Biomol. NMR*, **6**, 277–93 (1995).
89. Swain, S. and Atreya, H. S. *Open Magn. Reson. J.*, **1**, 95–103 (2008).
90. Kay, L. E., Keifer, P. and Saarinen, T. *J. Am. Chem. Soc.*, **114**, 10663–65 (1992).
91. Bartels, C., Xia, T. H., Billeter, M., Güntert, P. and Wuthrich, K. *J. Biomol. NMR*, **6**, 1–10 (1995).
92. Moseley, H. N. B., Monleon, D. and Montelione, G. T. *Nuclear Magnetic Resonance of Biological Macromolecules, Pt B*, **339**, 91–108 (2001).
93. Atreya, H. S. and Szyperski, T. *Proc. Natl. Acad. Sci. USA*, **101**, 9642–47 (2004).
94. Shen, Y., Atreya, H. S., Liu, G. and Szyperski, T. *J. Am. Chem. Soc.*, **127**, 9085–99 (2005).
95. Eletsy, A., Atreya, H. S., Liu, G. H. and Szyperski, T. *J. Am. Chem. Soc.*, **127**, 14578–79 (2005).
96. Liu, G. H., Aramini, J., Atreya, H. S., Eletsy, A., Xiao, R., Acton, T., Ma, L. C., Montelione, G. T. and Szyperski, T. *J. Biomol. NMR*, **32**, 261–61 (2005).
97. Barnwal, R. P., Rout, A. K., Chary, K. V. R. and Atreya, H. S. *J. Biomol. NMR*, **39**, 259–63 (2007).
98. Atreya, H. S., Garcia, E., Shen, Y. and Szyperski, T. *J. Am. Chem. Soc.*, **129**, 680–92 (2007).
99. Barnwal, R. P., Atreya, H. S. and Chary, K. V. R. *J. Biomol. NMR*, **42**, 149–54 (2008).
100. Barnwal, R. P., Rout, A. K., Atreya, H. S. and Chary, K. V. R. *J. Biomol. NMR*, **41**, 191–97 (2008).
101. Zhang, Q., Atreya, H. S., Kamen, D. E., Girvin, M. E. and Szyperski, T. *J. Biomol. NMR*, **40**, 157–63 (2008).
102. Swain, M. and Atreya, H. S. *J. Biomol. NMR*, **44**, 185–94 (2009).
103. Xia, Y. L., Zhu, G., Veeraraghavan, S. and Gao, X. L. *J. Biomol. NMR*, **29**, 467–76 (2004).
104. Xia, Y. L., Veeraraghavan, S., Zhu, Q. and Gao, X. L. *J. Magn. Reson.*, **190**, 142–48 (2008).
105. Wuthrich, K. *NMR of Proteins and Nucleic Acids*; Wiley, New York: NY, 1986.
106. Vuister, G. W. and Bax, A. *J. Am. Chem. Soc.*, **115**, 7772–77 (1993).
107. Montelione, G. T. and Wagner, G. *J. Am. Chem. Soc.*, **111**, 5474–75 (1989).
108. Bax, A., Vuister, G. W., Grzesiek, S., Delaglio, F., Wang, A. C., Tschudin, R. and Zhu, G. *Nuclear Magnetic Resonance, Pt C*, **239**, 79–105 (1994).
109. Dux, P., B., W., Boelens, R., Kaptein, R. and Vuister, G. W. *J. Biomol. NMR*, **10**, 301–06 (1997).
110. Barnwal, R. P., Jobby, M. K., Sharma, Y. and Chary, K. V. R. *J. Biomol. NMR*, **36**, 32–32 (2006).
111. Atreya, H. S., Sahu, S. C., Bhattacharya, A., Chary, K. V. R. and Govil, G. *Biochemistry*, **40**, 14392–403 (2001).
112. Karplus, M. *Journal of Physical Chemistry*, **85**, 2870–71 (1963).
113. Wishart, D. S. and Sykes, B. D. *J. Biomol. NMR*, **4**, 171–80 (1994).
114. Atreya, H. S., Sahu, S. C., Chary, K. V. R. and Govil, G. *J. Biomol. NMR*, **17**, 125–36 (2000).
115. Allegrozzi, M., Bertini, I., Janik, M. B. L., Lee, Y. M., Lin, G. H. and Luchinat, C. *J. Am. Chem. Soc.*, **122**, 4154–61 (2000).
116. Bertini, I., Donaire, A., Jimenez, B., Luchinat, C., Parigi, G., Piccioli, M. and Poggi, L. *J. Biomol. NMR*, **21**, 85–98 (2001).
117. Bertini, I., Luchinat, C. and Parigi, G. *Concepts in Magnetic Resonance*, **14**, 259–86 (2002).
118. Bertini, I., Janik, M. B. L., Lee, Y. M., Luchinat, C. and Rosato, A. *J. Am. Chem. Soc.*, **123**, 4181–88 (2001).
119. Banci, L., Bertini, I., Gori Savellini, G., Romagnoli, A., Turano, P., Cremonini, M. A., Luchinat, C. and Gray, H. B. *Proteins: Structure, Function, and Genetics*, **29**, 68–76 (1997).
120. Gardner, K. H., Rosen, M. K. and Kay, L. E. *Biochemistry*, **36**, 1389–401 (1997).
121. Nicholson, L. K., Kay, L. E., Baldisseri, D. M., Arango, J., Young, P. E., Bax, A. and Torchia, D. A. *Biochemistry*, **31**, 5253–63 (1992).
122. Gagne, S. M., Tsuda, S., Spyrapoulos, L., Kay, L. E. and Sykes, B. D. *J. Mol. Biol.*, **278**, 667–86 (1998).
123. Choy, W. Y. and Kay, L. E. *J. Biomol. NMR*, **25**, 325–33 (2003).
124. Werbelow, L. G. and Marshall, A. G. *J. Magn. Reson.*, **11**, 299–313 (1973).
125. Gardner, K. H., Konrat, R., Rosen, M. K. and Kay, L. E. *J. Biomol. NMR*, **8**, 351–56 (1996).
126. Rosen, M. K., Gardner, K. H., Willis, R. C., Parriss, W. E., Pawson, T. and Kay, L. E. *J. Mol. Biol.*, **263**, 627–36 (1996).
127. Zwahlen, C., Gardner, K. H., Sarma, S. P., Horita, D. A., Byrd, R. A. and Kay, L. E. *J. Am. Chem. Soc.*, **120**, 7617–25 (1998).
128. Tugarinov, V., Hwang, P. M., Ollerenshaw, J. E. and Kay, L. E. *J. Am. Chem. Soc.*, **125**, 10420–28 (2003).
129. Gross, J. D., Gelev, V. M. and Wagner, G. *J. Biomol. NMR*, **25**, 235–42 (2003).
130. Tugarinov, V., Hwang, P. M. and Kay, L. E. *Annual Review of Biochemistry*, **73**, 107–46 (2004).
131. Tugarinov, V. and Kay, L. E. *J. Biomol. NMR*, **28**, 165–72 (2004).
132. Atreya, H. S. and Chary, K. V. R. *J. Biomol. NMR*, **19**, 267–72 (2001).
133. Kay, L. E., Ikura, M., Zhu, G. and Bax, A. *Abstracts of Papers of the American Chemical Society*, **201**, 74–Anyl (1991).
134. Wishart, D. S., Sykes, B. D. and Richards, F. M. *Biochemistry*, **31**, 1647–51 (1992).
135. Wishart, D. S. and Case, D. A. *Methods Enzymol.*, **338**, 3–34 (2001).
136. Blechta, V. and Freeman, R. *Chemical Physics Letters*, **215**, 341–46 (1993).
137. Kupce, E. and Freeman, R. *J. Magn. Reson.*, **162**, 300–10 (2003).

138. Kupce, E. and Freeman, R. *J. Magn. Reson.*, **162**, 158–65 (2003).
139. Battiste, J. L. and Wagner, G. *Biochemistry*, **39**, 5355–65 (2000).
140. Jahnke, W. *ChemBioChem*, **3**, 167–73 (2002).
141. Linser, R., Chevelkov, V., Diehl, A. and Reif, B. *J. Magn. Reson.* **189**, 209–16 (2007).
142. Eletsky, A., Moreira, O., Kovacs, H. and Pervushin, K. *J. Biomol. NMR*, **26**, 167–79 (2003).
143. Wider, G. *Methods Enzymol.*, **394**, 382–98 (2005).
144. Pervushin, K., Vogeli, B. and Eletsky, A. *J. Am. Chem. Soc.*, **124**, 12898–902 (2002).
145. Schanda, P. and Brutscher, B. *J. Magn. Reson.*, **178**, 334–39 (2006).
146. Schanda, P., Kupce, E. and Brutscher, B. *J. Biomol. NMR*, **33**, 199–211 (2005).
147. Gal, M., Schanda, P., Brutscher, B. and Frydman, L. *J. Am. Chem. Soc.*, **129**, 1372–77 (2007).
148. Schanda, P. and Brutscher, B. *J. Am. Chem. Soc.*, **127**, 8014–15 (2005).
149. Schanda, P., Van Melckebeke, H. and Brutscher, B. *J. Am. Chem. Soc.*, **128**, 9042–43 (2006).
150. Kern, T., Schanda, P. and Brutscher, B. *J. Magn. Reson.*, **190**, 333–38 (2008).
151. Arnerio, C., Schanda, P., Dura, M. A., Ayala, I., Marion, D., Franzetti, B., Brutscher, B. and Boisbouvier, J. *J. Am. Chem. Soc.*, **131**, 3448–+ (2009).
152. Ross, A., Salzmann, M. and Senn, H. *J. Biomol. NMR*, **10**, 389–96 (1997).
153. Macura, S. *J. Am. Chem. Soc.*, **131**, 9606–07 (2009).
154. Mishkovsky, M., Kupce, E. and Frydman, L. *J. Chem. Phys.*, **127** (2007).
155. Tal, A., Shapira, B. and Frydman, L. *Angew. Chem. Int. Ed.*, **48**, 2732–36 (2009).
156. Frydman, L., Lupulescu, A. and Scherf, T. *J. Am. Chem. Soc.*, **125**, 9204–17 (2003).
157. Shapira, B., Lupulescu, A., Shrot, Y. and Frydman, L. *J. Magn. Reson.*, **166**, 152–63 (2004).
158. Shapira, B., Morris, E., Muszkat, K. A. and Frydman, L. *J. Am. Chem. Soc.*, **126**, 11756–57 (2004).
159. Shrot, Y., Shapira, B. and Frydman, L. *J. Magn. Reson.*, **171**, 163–70 (2004).
160. Mishkovsky, M., Gal, M. and Frydman, L. *J. Biomol. NMR*, **39**, 291–301 (2007).
161. Shrot, Y. and Frydman, L. *J. Magn. Reson.*, **195**, 226–31 (2008).
162. Gal, M., Melian, C., Demco, D. E., Blumich, B. and Frydman, L. *Chem. Phys. Lett.*, **459**, 188–93 (2008).
163. Shrot, Y. and Frydman, L. *J. Chem. Phys.*, **128** (2008).
164. Sun, Z. Y. J., Hyberts, S. G., Rovnyak, D., Park, S., Stern, A. S., Hoch, J. C. and Wagner, G. *J. Biomol. NMR*, **32**, 55–60 (2005).
165. Mobli, M., Maciejewski, M. W., Gryk, M. R. and Hoch, J. C. *Nature Methods*, **4**, 467–68 (2007).
166. Mobli, M. and Hoch, J. C. *Concepts Magn. Reson. A*, **32A**, 436–48 (2008).
167. Hoch, J. C., Maciejewski, M. W. and Filipovic, B. *J. Magn. Reson.*, **193**, 317–20 (2008).
168. Maciejewski, M. W., Qui, H. Z., Rujan, I., Mobli, M. and Hoch, J. C. *J. Magn. Reson.*, **199**, 88–93 (2009).
169. Meng, X., Nguyen, B. D., Ridge, C. and Shaka, A. *J. Magn. Reson.*, **196**, 12–22 (2009).
170. Staykova, D. K., Fredriksson, J., Bermel, W. and Billeter, M. *J. Biomol. NMR*, **42**, 87–97 (2008).
171. Szyperski, T., Fernandez, C. and Wüthrich, K. *J. Magn. Reson.*, **128**, 228–32 (1997).
172. Szyperski, T., Banecki, B., Braun, D. and Glaser, R. *J. Biomol. NMR*, **11**, 387–405 (1998).
173. Brutscher, B., Simorre, J. P., Caffrey, M. S. and Marion, D. *J. Magn. Reson. Series B*, **105**, 77–82 (1994).
174. Simorre, J. P., Caffrey, M., Brutscher, B., Morelle, N., Cordier, F. and Marion, D. *Journal of Cellular Biochemistry*, 76–76 (1995).
175. Kim, S. and Szyperski, T. *J. Biomol. NMR*, **28**, 117–30 (2004).
176. Barnwal, R. P., Rout, A. K., Chary, K. V. R. and Atreya, H. S. *Open Magn. Reson. J.*, **1**, 16–28 (2008).
177. Kupce, E. and Freeman, R. *J. Am. Chem. Soc.*, **125**, 13958–59 (2003).
178. Kupce, E. and Freeman, R. *J. Biomol. NMR*, **28**, 391–95 (2004).
179. Kupce, E. and Freeman, R. *J. Am. Chem. Soc.*, **128**, 6020–21 (2006).
180. Kupce, E., Nishida, T. and Freeman, R. *Prog. NMR Spectrosc.*, **42**, 95–122 (2003).



Hanudatta S. Atreya. b. 1974. M.Sc. 1997, Ph.D. 2002 (Chemistry) from Tata Institute of Fundamental Research (TIFR), Mumbai. Then, postdoctoral fellow at State University of New York at Buffalo, USA (2002–2006). Currently at Indian Institute of Science as Assistant Professor. Authored approximately 35 peer review publications and one US patent. Research interests in development and application of new NMR methodologies for studying structure, function and dynamics in biomolecules.